

Research Journal of Information Technology

ISSN 1815-7432



Research Journal of Information Technology 6 (2): 110-123, 2014 ISSN 1815-7432 / DOI: 10.3923/rjit.2014.110.123 © 2014 Academic Journals Inc.

Validation of Various Standard Strategies for Fluorescence Image Denoising of Cardiac Fibroblast Cells

¹K. Sampath Kumar and ²C. Arun

¹Department of Electronics and Communication Engineering, Sree Sastha College of Engineering, Chennai, India

²Department of Electronics and Communication Engineering, R.M.K. College of Engineering and Technology, Chennai, India

Corresponding Author: K. Sampath Kumar, Department of Electronics and Communication Engineering, Sree Sastha College of Engineering, Chennai, India

ABSTRACT

Fluorescence microscopy imaging is a common biomedical tool for researchers make use in the study of active processes occurring inside live cells. Although fluorescent confocal microscopes are consistent instruments, the acquired images are normally corrupted by a severe type of poisson noise owing to the small amount of acquired radiation (low photon-count images) and also the huge opto-electronics amplification. These effects are still more destructive when very low intensity incident radiation is employed to avoid photo toxicity. To validate various standards of denoising algorithms to denoising the cardio fibroblast cells, in which all the fluorescence images are affected by Poisson Gaussian noise. These images are considered especially as a cardio fibroblasts contribute to structural, biochemical, mechanical and electrical properties of the myocardium. The denoising approaches employed here can directly act on Poisson noise like PURELET or use approaches wherein Gaussianize the noise by means of standard VST algorithms and then Gaussian denoising algorithms like BLS_GSM, BM3D and OWT SURELET are proposed. The experimental results are carried out on how the ISNR changes with the change in algorithms and inverse transforms for cardio fibroblasts.

Key words: Cardiac fibroblast, fluorescence microscopy imaging, Gaussian denoising algorithms

INTRODUCTION

Fluorescence live-cell imaging is generally used to study intracellular molecular dynamics. In live cell microscopic imaging there is always exists a compromise between image quality and cell viability (Kumar and Arun, 2011). The prerequisite to image rapidly and in numerous dimensions, to capture dynamic intracellular procedures also constrains illumination and exposure regimes and requires fast camera readout. This is in turn results in low Signal to Noise Ratio (SNR) fluorescence images with mixed Poisson-Gaussian noise. Under such conditions effective denoising techniques are indispensable and become a critical tool to improve quantitative investigation of these images in order to understand dynamic intracellular processes and their fundamental mechanisms. In this study, an efficient approach is proposed to determine the impact of various standards of denoising approach on fluorescence images.

Cardiac fibroblast cells structured one of the largest cell populations, in terms of cell numbers, in the heart. However, they are frequently disregarded by *in vivo* and *in vitro* studies into cardiac

function. Fibroblasts give to cardiac development, myocardial structure, cell signaling and electro-mechanical function in healthy and diseased myocardium. Cardiac fibroblasts are significant determinants of both structure and function of the myocardium. They add to structural, biochemical, mechanical and electrical characteristics of cardiac function. Heart failure affects over all 14 million people worldwide and is a primary cause of death in adults and in children. Because postnatal cardiomyocytes (CMs) have small or no regenerative ability, current therapies are restricted. Fibroblast cells also lead to a new generation of reprogramming proficiency which involves trans-differentiating one adult somatic cell type directly into another (Anscombe, 1948). We reported direct reprogramming of fibroblasts into CM-like cells in vitro. The cardiac fibroblasts may reprogram more fully in vivo in their native environment which might encourage survival, maturation and pairing with adjacent cells. If so, the vast pool of cardiac fibroblasts in the heart could serve as an endogenous source of new CMs for regenerative therapy. Considering the importance of cardio fibroblasts we reflect on various denoising strategies for diminution of noise in the images which could lead to some life saving observations. Taking into consideration the potential of fibroblasts consider denoising these images and validate them using some standard denoising strategies. The methods considered either work on the Poisson noise or they Gaussianize the Poisson process and then denoise the Gaussianized image (Fryzlewicz and Nason, 2004).

For Gaussianizing the image process the variance stabilizing transform (VST) by applying the Anscombe root transformation:

$$f: z \to 2\sqrt{z+\frac{3}{8}}$$

to the data which will Gaussianize the noise which is then removed by means of a conventional denoising algorithm for additive white Gaussian noise which in this case is OWT_SURELET and BLS_GSM algorithms. An inverse transformation is applied to the denoised signal, obtaining the estimation of the signal of interest.

Proper inverse transformation is fundamental in order to diminish the bias error which arises when the nonlinear forward transformation is applied. Both the algebraic inverse and the asymptotically unbiased inverse proposed by Anscombe (1948) lead to a significant bias at low counts.

Also learn the effect of the PURELET algorithm where PURE is an unbiased, defined in the Haar wavelet domain (Kolaczyk and Dixon, 2000) of the mean-squared error between the original image and the estimated image. PURE-LET estimates the true image from the noisy image by minimizing PURE.

THEORY

Poisson noise: Let z_i , $i = 1, \ldots, N$, be the observed pixel values attained by an image acquisition device. Let us consider each z_i to be a self-governing random Poisson variable whose mean $y_i \ge 0$ is the fundamental intensity value to be anticipated. Clearly, the discrete Poisson probability of each z_i is:

$$E\{Zi \mid yi\} = \frac{yi^{zi}e^{-yi}}{zi!}$$
 (1)

As well to being the mean of the Poisson variable z_i, the parameter y_i is also its variance:

$$E\{Zi \mid yi\} = yi = var\{zi \mid yi\} \tag{2}$$

Poisson noise can be defined as:

$$\eta i = z i - E\{z i \mid y i\} \tag{3}$$

Therefore, trivially have $E\{\eta i \mid yi\} = 0$ and $var\{\eta i \mid yi\} = var\{zi \mid yi\} = yi$. In view of the fact that the noise variance reliant on the true intensity value, Poisson noise is depend on the signal. More purposely, the standard deviation of the noise ηi equals \sqrt{yi} . Owing to this, the effect of Poisson noise increases (i.e., the signal-to-noise ratio decreases) as the intensity value decreases.

Variance stabilization and the anscombe transformation: The underlying principle behind applying a variance-stabilizing transformation is to remove the data-dependence of the noise variance, as a result that it becomes constant throughout the entire data zi, i = 1,, N. Furthermore, if the transformation is besides normalizing (i.e., it results in a Gaussian noise distribution), can calculate approximately the intensity values yi with a conventional denoising technique designed for additive white Gaussian noise. Neither exact stabilization nor exact normalization is possible then, in actual fact, approximate or asymptotical results are used.

One of the most accepted variance-stabilizing transformations is the Anscombe transformation (10):

$$f: z \to 2\sqrt{z + \frac{3}{8}} \tag{4}$$

By (4) to Poisson distributed data provides a signal whose noise is asymptotically additive standard normal. The denoising of f(z) produces a signal D which is an estimate of $E\{f(z)|y\}$.

DENOISING

Gaussian denoising

Gaussian denoising-BLS-GSM: This approach is for removing noise from digital images, is depend on a numerical model of the coefficients of an over absolute multiscale oriented origin. Neighborhoods of coefficients at neighboring positions and scales are represented as the product of two self-governing arbitrary variables: a Gaussian vector and a hidden positive scalar multiplier. Beneath this model, the Bayesian least squares calculate each of coefficients which reduce to a weighted average of the local linear estimates over all potential values of the hidden multiplier variable (Zhang et al., 2008; Lefkimmiatis et al., 2009). The process of image denoising uses the same top-level formation as:

- Decompose the image into pyramid sub bands at different scales and orientations
- Denoise each sub band, apart from the low pass residual band
- Invert the pyramid transform, obtaining the denoised image

A vector related to a neighborhood of observed coefficients of the pyramid illustration can be defined as:

$$y = x + w = \sqrt{zu} + w \tag{5}$$

Observe that the assumed GSM structure of the coefficients, coupled through the assumption of independent additive Gaussian noise, means that the three random variables on the right side of (5) are self-determining.

Both u and w are zero-mean Gaussian vectors, with related covariance matrices Cu and Cw. The density of the observed neighborhood vector conditioned on a zero-mean Gaussian by way of covariance C(y|z) = zCu+Cw:

$$p(y \mid z) = \exp\left(\frac{-y^{T}(zCu + Cw)^{T}y}{\frac{2}{\sqrt{(2\pi)^{N} \|zCu + Cw\|}}}\right)$$
(6)

The neighborhood noise covariance Cw, is obtained by decomposing a delta function $\sigma\sqrt{NyNx}\delta(n,m)$ into pyramid sub bands where, (Ny, Nx) are the image dimensions. Elements of Cw may then be calculated directly as sample covariance. This process is simply generalized for nonwhite noise, by replacing the delta function with the inverse Fourier transform of the square root of the noise power spectral density. For given Cw, the signal covariance can be computed from the observation covariance matrix Cy. Compute from C(y|z) by taking expectations over z:

$$C(y) = E\{z\}Cu+Cw$$

Without loss of generality, set $E\{z\} = 1$, resulting in:

$$Cu = Cy - Cw \tag{7}$$

Bayes least squares estimator: For each neighborhood, need to estimate x_o , the reference coefficient at the middle of the neighborhood, from the set of observed (noisy) coefficients. The Bayes Least Squares (BLS) estimate is presently the conditional mean:

$$E\{x_c \mid y\} = \int x_c p(x_c \mid y) dx_c$$

$$= \iint_0^\infty x_c p(x_c, z \mid y) dz dx_c$$

$$= \iint_0^\infty x_c p(x_c \mid y, z) p(z \mid y) dz dx_c$$

$$\int_0^\infty p(z \mid y) E\{x_c \mid y, z\} dz$$
(8)

where also even assume the convergence in order to change the order of integration. Moreover, describe about each of these individual components.

Local wiener estimate: The main advantage of the GSM model is that the coefficient neighborhood vector x is Gaussian when conditioned on z. The fact that, coupled with the assumption of additive Gaussian noise means that the expected value inside the integral of (8) is merely a local linear (Wiener) estimate, were for the full neighborhood vector as:

$$E\{x \mid y, z\} = zC_{n}(zC_{n} + Cw)^{-1}y$$
(9)

By solving:

$$E\{x \mid y, z\} = \sum_{n=1}^{N} \frac{z m_{en} \lambda_n v_n}{z \lambda_n + 1}$$

$$\tag{10}$$

Posterior distribution of the multiplier: The other module of the solution given in (8) is the distribution of the multiplier, conditioned on the observed neighborhood values. Bayes' rule is used to compute this:

$$p(z|y) = \frac{p(y|z)p_z(z)}{\int_0^\infty p(y|a)p_z(a)da}$$
(11)

The proposed denoising algorithm as follows:

- Decompose the image into sub bands
- For each sub band (except the low pass residual):
 - Compute neighborhood noise covariance, C_w, from the image-domain noise covariance.
 - Estimate noisy neighborhood covariance, C_y
 - Estimate C_u from C_y and C_w using (7)
 - Compute Λ and M
 - · For each neighborhood
 - For each value z in the integration range:
- Compute $E\{x_c|y, z\}$ using (10)
- Compute p(y|z)
 - Compute (z|y) using (11)
 - Compute E{x_x|y} numerically using (8)
- Reconstruct the denoised image from the processed sub bands and the low pass residual to get D

Gaussian denoising OWT_SURELET: In SURE, no a priori image model is needed to optimize the denoising process which then purely amounts to solving a linear system of equations in each wavelet sub band (Luisier *et al.*, 2010). The general denoising approach comprises of expressing the denoising process, F(y) as a linear combination (LET: Linear expansion of thresholds) of given elementary processes, $F_k(y)$:

$$F(y) = \sum_{k=1}^{k} akFk(y) \tag{12}$$

At this point, the unknown weights ak are specific by minimizing the SURE. It is also likely, to evaluate the performance of the algorithm, to compare the result with what the minimization of the MSE would supply.

The linearity (12) is a vital advantage for solving the minimization problem, since the SURE is quadratic in F(y). The coefficients ak are, thus, the solution of a linear system of equations:

$$\frac{\sum_{k=1}^{k} Fk(y)^{T} Ft(y)at = Fk(y)^{T} y - \sigma^{2} div\{Fk(y)\}}{[M]k, 1 \quad [c]k \quad \text{for } k = 1, 2, ...K} Ma = c$$
(13)

This approach suggests that, a set of dissimilar denoising algorithms are also preferably selected with balancing denoising behaviors and optimize a weighting of these algorithms to obtain the best of them at once.

Point wise SURE-LET transform denoising: Initially, define a couple of linear transformations D-decomposition and R is the reconstruction such that RD = Identity: Typically D is a bank of decimated or undecimated filters. Once the size of the input and output data are frozen, these linear operators are characterized by matrices, respectively $D = (di, j)_{i,j \in [1:L] \times [1:N]}$ and $R = (ri, j)_{i,j \in [1:L] \times [1:N]}$ that satisfy the perfect reconstruction property RD = ID. Then, the whole denoising process boils down to the following steps.

- Apply D to the noisy signal y = x+b to get the transformed noisy coefficients $w = Dy = ((wi))_{i \in [1:L]}$
- Apply a point wise thresholding function $(\theta i(wi))_{i \in [1L]}$
- Revert to the original domain by applying R to the thresholded coefficients $\theta(w)$, yielding the denoised estimate $\hat{x} = R\theta(w)$

This algorithm can be summarized as a function of the noisy input coefficients:

$$\hat{\mathbf{x}} = \mathbf{F}(\mathbf{y}) = \mathbf{R}\mathbf{\theta}(\mathbf{D}\mathbf{y}) \tag{14}$$

The SURE-LET approach recommends that expressing F as a linear expansion of denoising algorithms Fk, according to:

$$F(y) = \frac{\sum_{k=1}^{K} akR\theta k(Dy)}{Fk(y)}$$
(15)

where, $\theta k(.)$ are the elementary point wise thresholding functions. This linear parameterization does not entail a linear denoising; certainly, the thresholding functions can be chosen as a nonlinear function.

A point wise thresholding function is possible to be efficient if it satisfies the following properties such as differentiability, anti-symmetry and linear behavior for large coefficients. A fine selection has been experimentally establish to be:

$$\theta i(w) = ai$$
, $1t1(w)+ai$, $2t2(w)$

Where:

$$t1(w) = w$$
 and $t2(w) = w(1 - e^{-(\frac{w}{3\sigma})^8})$

in each band i.

Summary of the algorithm:

- · Perform a boundary extension on the noisy image
- · Perform an UWT on the extended noisy image
- For i=1...J (number of band pass sub bands), For k=1, 2
 - Apply the point wise thresholding functions defined in (16) to the current sub band wi.
 - · Reconstruct the processed sub band by setting all the other sub bands to zero to obtain Fi, k(y)
 - Compute the first derivative of tk for each coefficient of the current sub band wi and build the corresponding coordinate of c as
 exemplified by Eq. 13

 $_{
m end}$

Gaussian denoising BM3D: The procedure is a transform domain enhanced sparse representation denoising method. Block Matching and 3-Dimensional filtering (BM3D) can achieve a high level of sparse representation of the noise free signal; therefore, the noise can be set independently from signal by shrinkage. In this way, the transform displays all the tiny details of image by grouped fractions simultaneously the essential unique feature of each individual fragment is protected (Portilla *et al.*, 2003).

The general idea of the BM3D denoising algorithm is the following:

- Block-wise estimates: For each block in the noisy image the filter performs:
 - **Grouping:** Finding blocks that are similar to the presently processed one and then stacking them together in a 3-D array (group)
 - Collaborative filtering: Applying a 3-D transform to the formed group, attenuating the noise by shrinkage (e.g., hard-thresholding) of the transform coefficients, inverting the 3-D transform to produce estimates of all grouped blocks and then returning the estimates of the blocks to their original places. Because the grouped blocks are similar, Block Matching and 3-Dimensional filtering (BM3D) can achieve a high level of sparse representation of the noise-free signal, thus, the noise can be set apart well from signal by shrinkage
- **Aggregation:** The output image is estimated by weighted averaging of all achieved block estimates that have overlap

Poisson denoising

Poisson Denoising PURELET: The fundamental theory behind this is to find a statistical approximation of the Mean Square Error (MSE), or "risk", between the (unknown) noiseless image and the processed noisy image. Owing to the Poisson noise theory, referred to this outcome as the PURE; this is analogous to the Stein's Unbiased Risk Estimate (SURE) which holds for Gaussian statistics (Blu and Luisier, 2007).

The objective is Minimization of MSE estimate over a collection of acceptable denoising processes to find the best one, in the sense of the Signal-to-Noise Ratio (SNR) which is a common quantifier of restoration quality. The efficiency of the method stems from the use of a simple normalized Haar-wavelet transform and from the perception of LET the acceptable denoising processes are expressed as a linear combination of basic denoising processes, from which only the weights are unknown (Willett and Nowak, 2003).

In this weights that are then computed by minimizing the PURE, through the resolution of a easy linear system of equations. This means that all the parameters of the algorithm are adjusted totally by design, without the need of user key in. For each sub band, our restoration functions involve several parameters which offer more flexibility than standard single-parameter thresholding functions. Importantly, the thresholds are modified to local estimates of the (signal-dependent) noise variance (Willett, 2006).

Similarly to what has been proposed for SURE-based denoising we describe the denoising function as the Linear Expansion of Thresholds (LET) defined as:

$$F(y) = \sum_{k=1}^{K} akR\theta k(w, w^{-})$$

Where:

$$R\theta k(w, w^{-}) = Fk(y) \tag{16}$$

Linear parameterization, in which PURE turn out to be quadratic in the ak's. Hence, the search for the optimal (in the minimum PURE sense) vector of parameters $a = [a1, a2...ak]^T$ boils down to the solution of the following system of linear equations: For k = 1..K, have:

$$\frac{\sum\limits_{k=1}^{K}fk(y)^{T}fl(y)a=(y)^{T}f_{k}^{-}(y)-\sigma^{2}div\left\{f_{k}^{-}(y)\right\}}{[M]k,1}$$
 [c]k

For k = 1, 2, ... K

$$Ma = c (17)$$

By means of the first-order Taylor-series approximation of PURE obtain a comparable system of linear equations given by:

$$\hat{\mathbf{c}} = [\mathbf{y}^{\mathrm{T}}(\mathbf{f}_{\nu}(\mathbf{y}) - \partial \mathbf{f}_{\nu}(\mathbf{y})) - \sigma^{2} \operatorname{div}\{\mathbf{f}_{\nu}(\mathbf{y}) - \sigma \mathbf{f}_{\nu}(\mathbf{y})\}] \ \mathbf{k} \in [1 \dots \mathbf{k}]$$

$$\tag{18}$$

Inverse transformation: Apply an inverse transformation to D in order to get hold of the desired estimate of y. The direct algebraic inverse of is:

$$Ia(D) f^{-1}(D) = \left(\frac{D}{2}\right)^2 - \frac{3}{8}$$
 (19)

but the consequential measure of y is biased, because the nonlinearity of the transformation f means generally have:

$$\mathbb{E}\{f(z)|y\} \neq f(\mathbb{E}\{z|y\}) \tag{20}$$

and therefore:

$$f^{-1}(E\{f(z)|y\}) \neq E\{z|y\}$$
 (21)

Another possibility is to use the adjusted inverse:

$$Ib(D) = \left(\frac{D}{2}\right)^2 - \frac{1}{8}$$
 (22)

which provides asymptotical unbiasedness for large counts. This is the inverse typically used in applications.

While the asymptotically unbiased inverse (22) provides good results for high-count data, applying it to low-count data leads to a biased estimate.

Exact unbiased inverse: Provided a successful denoising, i.e., D is treated as $E\{f(z)|y\}$, the exact unbiased inverse of the Anscombe transformation Ic f is an inverse transformation that maps the values $E\{f(z)|y\}$ to the desired values $E\{z|y\}$:

$$Ic: E\{f(z)|y\} \rightarrow E\{z|y\} \tag{23}$$

As $E\{z|y\} = y$ for any given y, the drawback of finding the inverse Ic reduces to computing the values $E\{f(z)|y\}$ which is done by numerical evaluation of the integral corresponding to the expectation operator E:

$$E\{f(z) | y\} = \int_{-\infty}^{0} f(z)p(z | y)dz$$
 (24)

where p(z|y) is the generalized probability density function of z conditioned on y. In this case the discrete poisson probabilities p(z|y) were used so can replace the integral by summation:

$$E\{f(z) | y\} = \sum_{z=0}^{\infty} f(z)p(z | y)$$
 (25)

Additionally, since here f(z) is the forward Anscombe transformation that can be written (25) as:

$$E\{f(z) \mid y\} = 2\sum_{z=0}^{\infty} \left(\sqrt{z + \frac{3}{8} \cdot \frac{y^z e^{-y}}{z!}} \right)$$
 (26)

Let us state that if the exact unbiased inverse (23) is applied to the denoised data D with some errors (in the sense that $D \neq E\{f(z)|y\}$, then the estimation error y = lc(D) an comprise variance with bias components. In general, the unbiasedness of Ic holds only provided that $D = E\{f(z)|y\}$ exactly, as it is assumed.

EXPERIMENTS

All the experiments consist of both the Gaussian based denoising strategies and poisson based denoising strategy. To implement the exact unbiased inverse Ic in practice, it is sufficient to compute (26) for a limited set of values y; for arbitrary values of y then use linear interpolation based on these measured values of (26) and for large values of y approximate Ic through Ib. Also compute the PURELET approach for the same images. The performances of these algorithms are evaluated by the peak signal-to-noise ratio (PSNR). The PSNR is calculated using the Eq:

$$10\log_{10}\left(\frac{\max(yi)^2}{\sum_{i}((\hat{y}l - yi^2 \mid N))}\right) \tag{27}$$

where N is the total number of pixels in the image.

RESULTS

The test images used in the experiments are below.

The test images used for this experiment were shown in Fig. 1, 2, 3, 4, 5 and 6 and evaluate the performance in terms of PSNR. The approaches used here are the OWT-SURELET, BLS_GSM, BM3D and PURELET for the denoising and the inversion is done with either the exact unbiased inverse or the asymptotically unbiased inverse.

The denoising performance is evaluated in terms of PSNR. Table 1 shows the results of BLS_GSM. Table 2 shows the results of OWT-SURELET. Table 3 shows the results of BM3D and Table 4 shows the results using PURELET. The plots of the PSNR values obtained using BLS_GSM, OWT SURELET and PURELET at a glance shows that PURELET and BLS_GSM provide more regular performances when compared to the other two strategies in general for cardio fibroblasts.

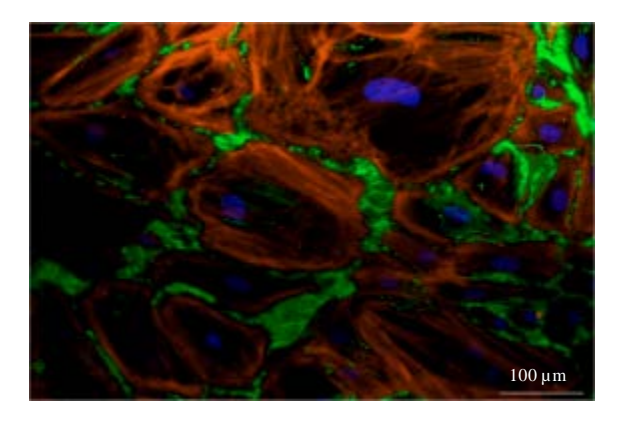


Fig. 1: Adult human heart cultured in confluent state allowing for ECM deposition

Res. J. Inform. Technol., 6 (2): 110-123, 2014

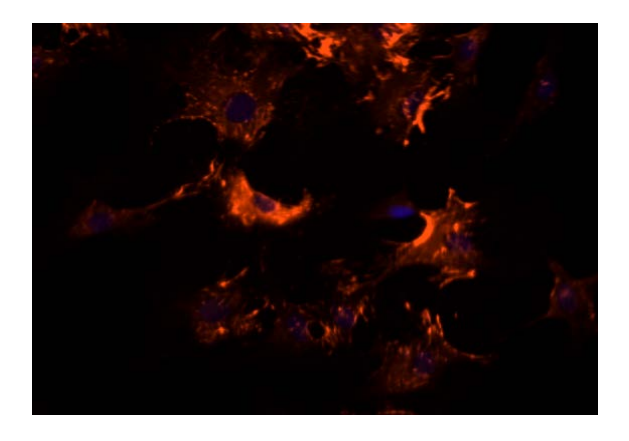


Fig. 2: Rat Cardiac Fibroblasts (RCF) provided by Innoprot isolated from sprague

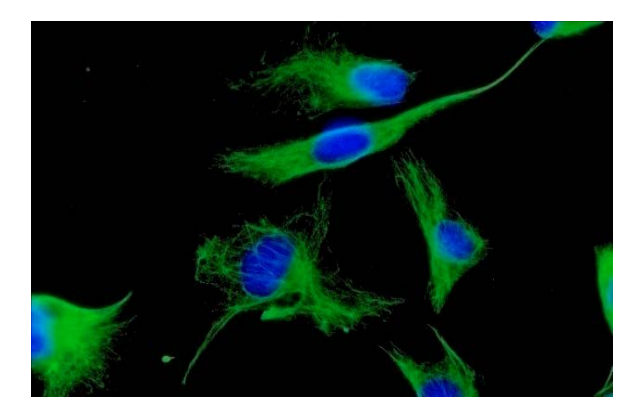


Fig. 3: Human Cardiac Fibroblasts (HCF)-immunostaining for fibronectin, 100x

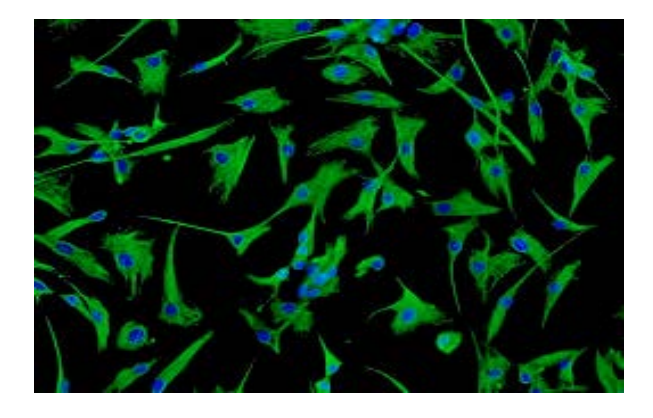


Fig. 4: Human Cardiac Fibroblasts-adult atrial (HCF-aa)-Relief contrast, 200x

Res. J. Inform. Technol., 6 (2): 110-123, 2014

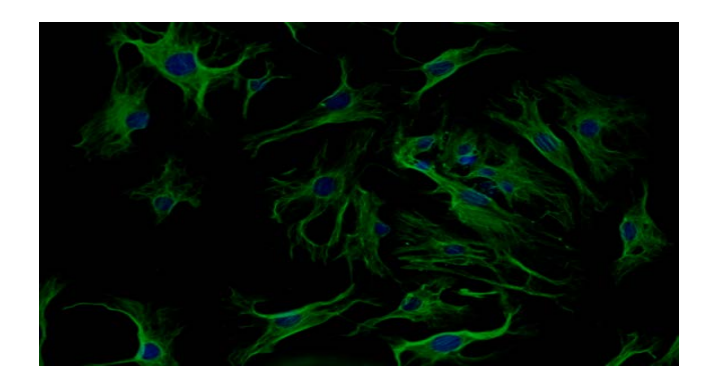


Fig. 5: Mouse Cardiac Fibroblasts (MCF)

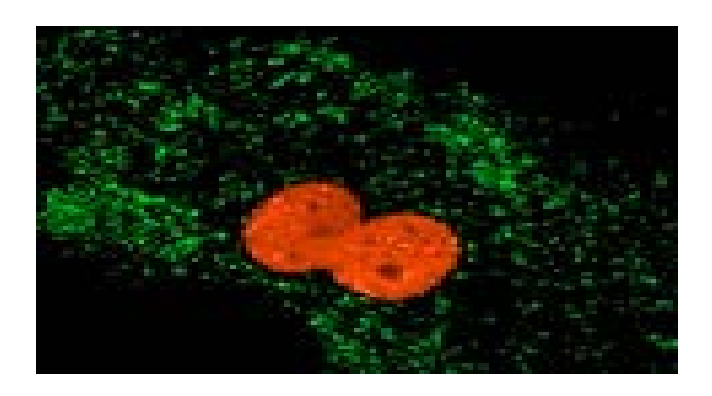


Fig. 6: Mouse Cardiac Fibroblasts (MCF)-Phase contrast, 100x

Table 1: Test results using BLS-GSM $\,$

	Figure 1		Figure 2		Figure 3		Figure 4		Figure 5		Figure 6	
Images	ISNR	ISNR	ISNR	ISNR	ISNR	ISNR	ISNR	ISNR	ISNR	SNR	ISNR	ISNR
σ	ASYIN	EUINV	ASYIN	EUINV	ASYIN`	EUINV	ASYIN	EUINV	ASYIN	EUINV	ASYIN	EUINV
1	34.5654	34.5653	41.6428	41.6422	37.8428	37.8531	37.9952	38.0036	39.6865	39.6923	41.1431	41.1550
2	29.4393	29.4393	37.2229	37.2222	31.0561	31.0581	30.1327	30.1338	35.7140	35.7146	30.3146	30.3154
5	24.9042	24.9042	31.6840	31.6837	28.5991	28.6002	24.7699	24.7702	30.1588	30.1586	22.4679	22.4680
10	21.9601	21.9601	26.9561	26.9561	25.7441	25.7448	22.0206	22.0208	25.8725	25.8724	21.2964	21.2965
15	20.1473	20.1473	23.9288	23.9288	23.5622	23.5626	20.5237	20.5238	23.1554	23.1554	20.4956	20.4956
20	18.6603	18.6602	21.6706	21.6706	21.7441	21.7443	19.3212	19.3212	21.1499	21.1498	19.5207	19.5207
25	17.4140	17.4140	19.8794	19.8794	20.2357	20.2358	18.4129	18.4129	19.4554	19.4554	18.4913	18.4913

Table 2: Test results using BLS-GSM $\,$

	Figure 1		Figure 2		Figure 3		Figure 4		Figure 5		Figure 6	
Images	ISNR	ISNR	ISNR	ISNR	ISNR	ISNR	ISNR	ISNR	ISNR	SNR	ISNR	ISNR
σ	ASYIN	EUINV	ASYIN	EUINV	ASYIN	EUINV	ASYIN	EUINV	ASYIN	EUINV	ASYIN	EUINV
1	25.7181	25.7174	20.6224	20.6219	46.7551	46.8816	46.4218	46.4831	46.1928	6.2214	46.3353	46.3773
2	10.2719	10.2718	-0.7081	-0.7081	41.4257	41.4612	41.2272	41.2434	41.0873	1.0897	41.1747	41.1852

Res. J. Inform. Technol., 6 (2): 110-123, 2014

Table 2: Continue

	Figure 1		Figure 2		Figure 3		Figure 4		Figure 5		Figure 6	
Images	ISNR	ISNR	ISNR	ISNR	ISNR	ISNR	ISNR	ISNR	ISNR	SNR	ISNR	ISNR
σ	ASYIN	EUINV	ASYIN	EUINV	ASYIN	EUINV	ASYIN	EUINV	ASYIN	EUINV	ASYIN	EUINV
5	-22.5462	-22.5462	-32.9253	-32.9253	33.8798	33.8860	33.7914	33.7941	33.7277	33.7272	33.7676	33.7693
10	-43.7697	-43.7697	-58.7133	-58.7133	27.9955	27.9971	27.9496	27.9504	27.9164	27.9163	27.9373	27.9377
15	-59.6547	-59.6547	-74.2782	-74.2782	24.5189	24.5196	24.4880	24.4883	24.4654	24.4654	24.4796	24.4798
20	-71.7144	-71.7144	-85.5547	-85.5547	22.0427	22.0431	22.0193	22.0195	22.0023	22.0023	22.0130	22.0131
25	-81.2521	-81.2521	-94.4419	-94.4418	20.1180	20.1183	20.0993	20.0994	20.0856	20.0856	20.0942	20.0943

Table 3: Test results using BM3D

Images o	Figure (BM3D)									
	1	2	3	4	5	6				
1	11.4163	5.6117	8.7798	7.8703	6.0967	6.7974				
2	6.9800	2.6525	7.9604	6.8301	4.5631	5.2761				
5	3.2937	0.2437	7.1867	5.1280	2.8780	3.5894				
10	2.0582	0.2434	6.6650	4.0626	1.3885	2.7446				
15	1.7767	0.2434	6.3493	3.6150	0.8184	2.3628				
20	1.6773	0.2434	6.1268	3.3263	0.3661	2.1032				
25	1.6320	0.2434	5.9379	3.1314	0.3659	1.9062				

Table 4: Test results using PURE-LET

Images σ	Figure (UWT PURELET)										
	1	2	3	4	5	6					
1	22.6255	31.1791	20.8908	8.3525	11.0595	43.7163					
2	22.4838	30.1113	35.7760	7.0933	16.5616	40.4506					
5	21.9430	26.9641	32.1599	3.2432	26.6556	33.8005					
10	20.8010	23.1698	27.4417	-3.3539	25.8080	28.0298					
15	19.5560	20.4871	24.2312	-10.1915	22.9631	24.5648					
20	18.3351	18.4292	21.8843	-25.3550	-4.4466	22.0833					
25	17.1897	16.7638	19.9718	-23.9359	9.3490	20.1567					

CONCLUSION

Results from the various denoising algorithms show that the BLS_GSM denoising and PURE-LET denoising provides stable performance when compared to BM3D and OWT-SURELET for almost all fibroblast images. OWT-SURELET approaches provide higher ISNR when the low sigma value. As the sigma value increases there is a sharp decrease in the signal to noise ratio. BM3D has shown variations which kept back fluctuating based on intensity of input images. They did not provide significant improvement in the SNR and showed poor performance as sigma increased. All algorithms show deterioration in SNR as sigma increased. The BLS_GSM and OWT-SURELET showed improvement when using the exact unbiased transform when compared to asymptotic inverse transform. The performance improvement gets slow when there is increase in sigma values. The total comparison of results shows that the PURELET BLS_GSM or OWT SURELET strategies can be used for low sigma values. As standard deviation increases it is better to stick on to BLS_GSM or PURELET strategy. Denoising strategies is an essential tool for cardio

fibroblast images as cardiac fibroblasts are important determinants for both structure and function of the myocardium. Cardio fibroblasts contribute to structural, biochemical, mechanical and electrical characteristics of cardiac function. They are sources and targets of bio-chemical and electro-mechanical signaling pathways. Future research focusing on cardiac fibroblasts will improve the understandability of cardiac function in normal and patho-physiological states. Therefore the study of denoising fibroblasts will be equally crucial for proper understanding of cardiac function.

REFERENCES

- Anscombe, F.J., 1948. The transformation of poisson, binomial and negative-binomial data. Biometrika, 35: 246-254.
- Blu, T. and F. Luisier, 2007. The SURE-LET approach to image denoising. IEEE Trans. Image Process., 16: 2778-2786.
- Fryzlewicz, P. and G.P. Nason, 2004. A Haar-Fisz algorithm for Poisson intensity estimation. J. Comput. Graphical Stat., 13: 621-638.
- Kolaczyk, E.D. and D.D. Dixon, 2000. Nonparametric estimation of intensity maps using Haar wavelets and Poisson noise characteristics. Astrophys. J., 534: 490-505.
- Kumar, K.S. and C. Arun, 2011. Poisson noise removal from flourescence images using optimized variance-stabilizing transformations and standard gaussian denoising strategies. Indian J. Applied Res., 1: 79-82.
- Lefkimmiatis, S., P. Maragos and G. Papandreou, 2009. Bayesian inference on multiscale models for Poisson intensity estimation: Applications to photon-limited image denoising. IEEE Trans. Image Process., 18: 1724-1741.
- Luisier, F., C. Vonesch, T. Blu and M. Unser, 2010. Fast interscale wavelet denoising of poisson-corrupted images. Signal Process., 90: 415-427.
- Portilla, J., V. Strela, M.J. Wainwright and E.P. Simoncelli, 2003. Image denoising using scale mixtures of Gaussians in the wavelet domain. IEEE Trans. Image Process., 12: 1338-1351.
- Willett, R.M. and R.D. Nowak, 2003. Platelets: A multiscale approach for recovering edges and surfaces in photon-limited medical imaging. IEEE Trans. Med. Imag., 22: 332-350.
- Willett, R.M., 2006. Multiscale analysis of photon-limited astronomical images. Proceedings of the 4th Conference Statistical Challenges in Modern Astronomy, Volume 371, June 12-15, 2006, Pennsylvania, USA.
- Zhang, B., J.M. Fadili and J.L. Starck, 2008. Wavelets, ridgelets and curvelets for Poisson noise removal. IEEE Trans. Image Proc., 17: 1093-1108.